Pharmaceutical Sciences and Drug Design
ISSN: 3062-4428
2024, Volume 4, Page No: 141-167

Available online at: www.galaxypub.co/page/journals

Galaxy Publication

Mechanistic Insights into Zuogui Jiangtang Shuxin Formula for Diabetic Cardiomyopathy: An Integrated Serum Pharmacochemistry and Network Pharmacology Study

Hiroshi Tanaka[1]*, Yuji Sato[1]

[1]Department of Phytochemistry, Faculty of Science, Kyoto University, Kyoto, Japan.

***E-mail** ✉ hiroshi.tanaka.jp@outlook.com

Received: 01 June 2024; **Revised:** 05 September 2024; **Accepted:** 09 September 2024

ABSTRACT

This research aimed to elucidate the mechanisms through which the Zuogui Jiangtang Shuxin formula (ZGJTSXF) alleviates diabetic cardiomyopathy (DCM) using a combined approach of serum pharmacochemistry, network pharmacology, and experimental validation.Following oral administration of ZGJTSXF in rats, serum compounds were analyzed using UPLC-Q-Exactive-Orbitrap-MS. A network linking bioactive components of ZGJTSXF to DCM-associated targets was established with Cytoscape. Functional enrichment analyses, including Gene Ontology and KEGG pathway assessments, were performed to identify critical molecular targets and signaling pathways. DCM model mice were treated with ZGJTSXF, and the predicted key pathways were validated through qPCR and Western blot assays.Analysis identified 78 serum compounds, including flavonoids, peptides, nucleosides, organic acids, phenylpropanoids, alkaloids, phenanthrenequinones, iridoids, phenols, and saponins. Network pharmacology indicated that ZGJTSXF may influence targets such as ALB, TNF, AKT1, GAPDH, VEGFA, EGFR, SRC, CASP3, MAPK3, JUN, and modulate the PI3K/AKT pathway in DCM. Administration of ZGJTSXF improved glucose metabolism, cardiac function, and myocardial tissue structure in DCM mice. Importantly, ZGJTSXF reduced cardiomyocyte apoptosis, which correlated with activation of the PI3K/AKT signaling pathway and increased levels of anti-apoptotic proteins Bcl-2 and Bcl-xL.These findings provide evidence that ZGJTSXF exerts cardioprotective effects in DCM via PI3K/AKT pathway activation and inhibition of apoptosis. The study also identifies the potential bioactive constituents responsible, offering a basis for future development of ZGJTSXF-based therapies for diabetic cardiomyopathy.

Keywords: Zuogui jiangtang shuxin formula, Diabetic cardiomyopathy, Network pharmacology, Serum pharmacochemistry, PI3K/AKT pathway, Apoptosis

How to Cite This Article: Tanaka H, Sato Y. Mechanistic Insights into Zuogui Jiangtang Shuxin Formula for Diabetic Cardiomyopathy: An Integrated Serum Pharmacochemistry and Network Pharmacology Study. Pharm Sci Drug Des. 2024;4:141-67. https://doi.org/10.51847/JWhQbzHz1v

Introduction

Diabetic cardiomyopathy (DCM) is a distinct cardiac disorder characterized by structural and functional abnormalities of the heart caused by diabetes mellitus (DM), independent of other cardiovascular risk factors [1]. According to the 10th edition of the International Diabetes Federation (IDF) Diabetes Atlas, approximately 537 million adults currently suffer from diabetes worldwide, and this number is projected to reach 700 million by 2045 [2]. With the rising prevalence of DM, the occurrence of DCM is also increasing. Studies indicate that DCM represents a leading cause of mortality among diabetic patients, accounting for roughly 50–80% of deaths in this population [3]. The pathogenesis of DCM is multifactorial, involving systemic metabolic disturbances, mitochondrial dysfunction, oxidative stress, microvascular impairment, inflammation, and adverse cardiac remodeling [4]. Despite advances in treatment, effective therapies remain limited [5]. While medications such as metformin can manage hyperglycemia, they carry risks including renal impairment, lactic acidosis in cases of

accumulation, and contraindications in certain comorbid conditions [6, 7]. Consequently, there is a pressing need for novel, effective, and safe therapeutic strategies for DCM.

Traditional Chinese Medicine (TCM) offers unique advantages due to its multi-component, multi-target, and multi-pathway characteristics, making it a promising approach for preventing and managing DM and its complications, including DCM [8]. Additionally, TCM is increasingly valued for its efficacy, affordability, and minimal side effects [8]. Zuogui Jiangtang Shuxin formula (ZGJTSXF), developed by Professor Chen Da Shun at Hunan University of Traditional Chinese Medicine, is composed of nine herbs, including Panax ginseng C. A. Meyer, Astragalus membranaceus (Fisch.) Bunge, Rehmannia glutinosa (Gaetn.) Libosch. ex Fisch. et Mey., Pueraria lobata (Willd.) Ohwi, Cornus officinalis Sieb. et Zucc., Salvia miltiorrhiza Bunge, Coptis chinensis Franch., Ophiopogon japonicus (Linn. f.) Ker-Gawl., and Crataegus pinnatifida Bge. ZGJTSXF is traditionally used to nourish Yin, benefit Qi, invigorate blood circulation, and remove toxins. Previous studies from our group demonstrated that ZGJTSXF improves glucolipid metabolism, reduces serum inflammatory factors, and protects the myocardium via anti-lipid peroxidation effects in MKR mice with type 2 diabetes [9, 10]. Nevertheless, the precise bioactive constituents and mechanisms by which ZGJTSXF exerts cardioprotective effects in DCM remain unclear, limiting its broader clinical application.

Given the complexity of TCM, it is widely accepted that only components absorbed into the bloodstream contribute to therapeutic effects [11]. Advanced analytical methods are therefore essential to uncover the interactions between TCM components and biological networks. Ultra high-performance liquid chromatography coupled with high-resolution mass spectrometry (UPLC-Q-Exactive-Orbitrap-MS) offers high sensitivity, resolution, and accuracy, making it a powerful tool for identifying TCM compounds [12]. Network pharmacology combines systems biology, pharmacology, computational biology, and network analysis to investigate interactions among drugs, targets, and diseases, providing a framework to decode complex TCM mechanisms [13]. Integrating UPLC-Q-Exactive-Orbitrap-MS with network pharmacology and bioinformatics allows systematic elucidation of the material basis and therapeutic mechanisms of TCM formulations.

In this study, we applied UPLC-Q-Exactive-Orbitrap-MS to identify active components in the serum of rats administered ZGJTSXF and integrated these findings with network pharmacology to predict potential targets. Gene and pathway enrichment analyses were further conducted to explore therapeutic mechanisms. Finally, a DCM mouse model was employed to validate the predicted biological pathways in vivo. This combined in silico and experimental approach **(Figure 1)** provides a comprehensive understanding of ZGJTSXF's material basis and mechanisms of action in treating DCM, offering insights for its clinical use and the development of novel therapies for diabetic cardiomyopathy.

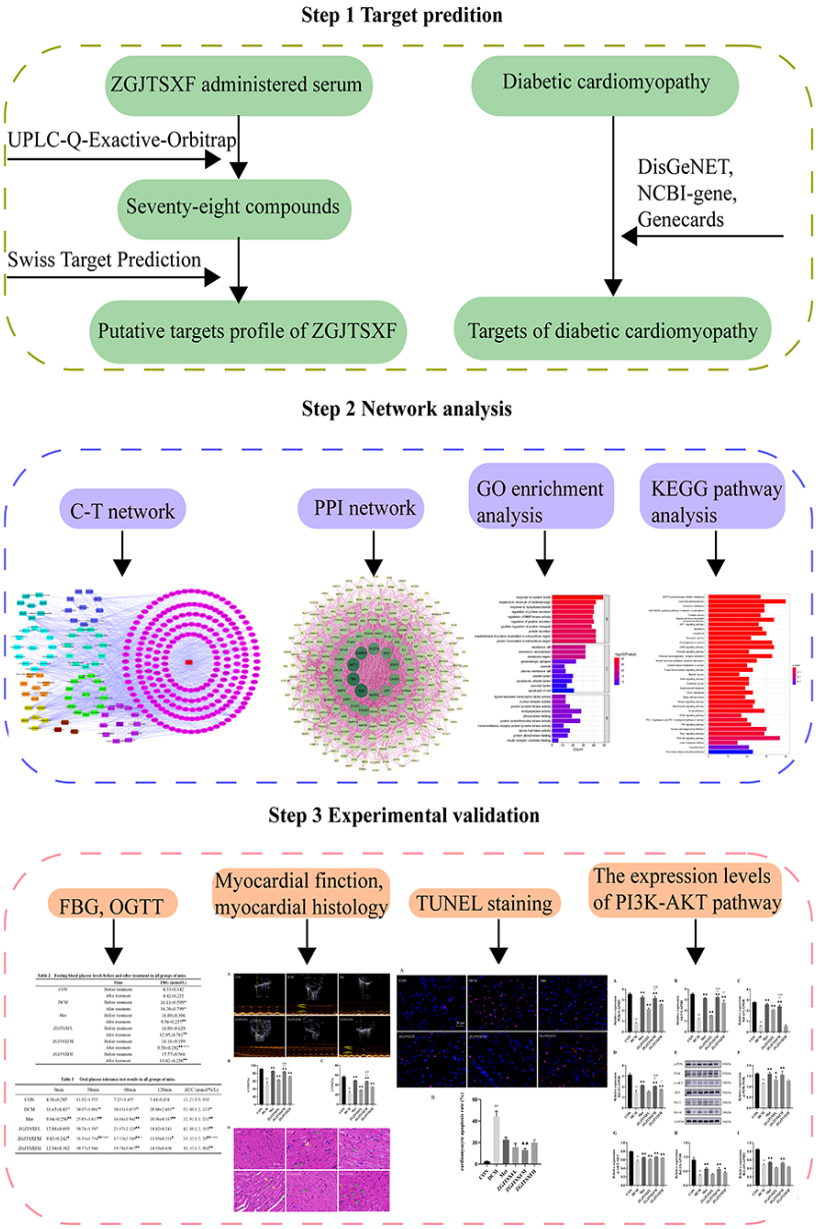

Figure 1. A schematic representation shows the outlines on studying the potential molecular mechanisms of action of Zuogui Jiangtang Shuxin formula (ZGJTSXF). The main active compounds of ZGJTSXF were identified by UPLC-Q-Exactive-Orbitrap-MS analysis of medicated rat serum. The potential targets for ZGJTSXF in treating DCM were also identified through analysis of multiple databases. The common targets were subjected to in silicon network pharmacology (C-T network and PPI network) analysis and pathway enrichment analysis. The mouse DCM model was established to experimentally validate the predicted targets and pathways through multiple cellular and molecular approaches.

The workflow of this study illustrates the approach used to investigate the potential molecular mechanisms underlying the effects of Zuogui Jiangtang Shuxin formula (ZGJTSXF). Active compounds absorbed into the bloodstream after oral administration of ZGJTSXF were identified using UPLC-Q-Exactive-Orbitrap-MS. Putative therapeutic targets for diabetic cardiomyopathy (DCM) were predicted by integrating data from multiple databases. Shared targets were further analyzed using in silico network pharmacology, including compound-target and protein-protein interaction (PPI) networks, followed by functional and pathway enrichment analyses. Finally, the predicted mechanisms were validated in a DCM mouse model through molecular and cellular experiments.

Materials and Methods

Experimental animals

Male Sprague-Dawley rats (average weight 240 ± 10 g) were obtained from Hunan SJA Laboratory Animal Co., Ltd. MKR mice, carrying a dominant-negative IGF-1 receptor in skeletal muscle as originally developed by Fernandez *et al*. [14], were provided by Dr. Derek LeRoith from the NIH Diabetes Research Center (Bethesda, MD, USA). Animals were housed under standard conditions (22 ± 2 °C, 50 ± 10% humidity) with free access to food and water in a specific pathogen-free facility at Hunan University of Traditional Chinese Medicine. Homozygous MKR mice were bred in-house, and their offspring were used for experiments. All protocols complied with the Basel Declaration and NIH guidelines, and were approved by the Ethics Committee of Hunan University of Chinese Medicine (Approval No. ZYFY20201229).

Serum collection and UPLC-Q-Exactive-Orbitrap-MS analysis

ZGJTSXF was procured from the herbal pharmacy of the First Affiliated Hospital of Hunan University of Traditional Chinese Medicine. Rats were randomly assigned to two groups: control (0.9% saline, n=10) and treatment (57.81 g/kg ZGJTSXF, n=10), with the dose corresponding to five times the clinical equivalent based on standard animal dose conversion [15]. The formulation was administered orally once daily for seven consecutive days. After a 12-hour fast, blood was collected via the abdominal aorta two hours post-administration. Serum was separated by centrifugation (12,000 rpm, 10 min, 4 °C). For analysis, 300 μL of serum was mixed with 900 μL methanol, vortexed for 10 minutes, centrifuged at 12,000 rpm for 15 minutes, and the supernatant was used for UPLC-Q-Exactive-Orbitrap-MS detection.

Chromatographic separation was performed on a Waters Xbridge BEH C18 column (2.1 × 100 mm, 2.6 μm) at 40 °C, with a flow rate of 0.3 mL/min and 10 μL injection volume. The mobile phase consisted of 0.1% formic acid in water (A) and 0.1% formic acid in acetonitrile (B), with the following gradient: 0–1.5 min, 2% B; 1.5–20 min, 2–45% B; 20–27 min, 45–95% B; 27–32 min, 95% B; 32–32.1 min, 95–2% B; 32.1–35 min, 2% B. Mass spectrometry data were acquired in positive and negative electrospray ionization modes, and processed using Xcalibur 4.3 and Compound Discoverer 3.2 (Thermo Fisher Scientific, USA).

Identification of potential targets and network construction

To determine potential targets of absorbed ZGJTSXF compounds, their SMILES structures were retrieved from PubChem and analyzed with SwissTargetPrediction (http://www.swisstargetprediction.ch/). DCM-related targets were collected from DisGeNET (https://www.disgenet.org/), NCBI Gene (https://www.ncbi.nlm.nih.gov/), and GeneCards (https://www.genecards.org/). Overlapping targets were used to construct a compound-target network in Cytoscape v3.7.2.

Protein-Protein Interaction (PPI) network

Shared targets were uploaded to the STRING database (https://string-db.org/cgi/input.pl) with “Homo sapiens” as the species and a minimum combined score >0.4. The resulting PPI network was visualized in Cytoscape, and network topology was analyzed using Network Analyzer. Genes with degree values exceeding twice the network average were designated as core targets.

Gene Ontology (GO) and KEGG pathway enrichment analysis

The overlapping targets of ZGJTSXF and DCM were subjected to functional enrichment analyses using the R packages ClusterProfiler, DOSE, and Pathview, following the developers’ protocols. Gene Ontology (GO) enrichment analysis and Kyoto Encyclopedia of Genes and Genomes (KEGG) pathway analysis were conducted to identify key biological processes and signaling pathways associated with ZGJTSXF’s therapeutic effects against DCM, with a significance threshold of $p \leq 0.05$.

Ethical considerations

All data utilized in this study were obtained from publicly accessible databases, including PubChem, Swiss Target Prediction, DisGeNET, NCBI-gene, GeneCards, and STRING. Since these resources provide open-access datasets for scientific research, formal ethics approval was not required. The Ethics Review Committee of the First Affiliated Hospital of Hunan University of Traditional Chinese Medicine confirmed that the study was exempt from ethical review.

Animal model and treatment protocols

Thirty male MKR mice (8 weeks old) were randomly allocated into five groups (n=6 per group): 1) DCM model group (DCM), 2) metformin treatment group (Met), 3) low-dose ZGJTSXF (ZGJTSXFL), 4) medium-dose ZGJTSXF (ZGJTSXFM), and 5) high-dose ZGJTSXF (ZGJTSXFH). DCM was induced by feeding mice a high-fat diet (60% kcal from fat; Jiangsu Xietong, XTHF60) for four weeks, followed by intraperitoneal injection of 1% streptozotocin (STZ; Sigma Aldrich, USA) at 40 mg/kg/day for five consecutive days, dissolved in citrate buffer (pH 4.5). Fasting blood glucose (FBG) levels were monitored regularly to confirm diabetes development. An additional six age- and sex-matched C57BL/6 mice served as healthy controls (CON).

The human therapeutic dose of ZGJTSXF was converted to equivalent mouse doses based on body surface area [15]. Treatment groups received daily gavage for four weeks as follows: Met group, 0.25 g/kg/day metformin (CSPC OUYI Pharmaceutical, China); ZGJTSXFL, 16.84 g/kg/day ZGJTSXF; ZGJTSXFM, 33.67 g/kg/day ZGJTSXF; ZGJTSXFH, 67.34 g/kg/day ZGJTSXF. CON and DCM groups received an equal volume of distilled water. After the final administration, mice were fasted for 12 h before tail vein blood collection, and FBG levels were measured using a GT-1980 glucose meter (Aikelai Medical Electronics, China). All procedures were approved by the Animal Ethical Committee of Hunan University of Chinese Medicine.

Glucose Tolerance Test (GTT)

One week prior to the end of treatment, glucose tolerance was evaluated. Mice were fasted overnight and administered a 2 g/kg glucose solution via oral gavage. Blood samples were collected from the tail vein at 0, 30, 60, and 120 minutes post-glucose load. Glucose concentrations were measured using a GT-1980 glucometer and compatible test strips (Sinocare Inc., Changsha, China). The area under the curve (AUC) for glucose response was calculated using the trapezoidal method.

Echocardiography

Cardiac function was assessed using a VINNO 6 high-resolution ultrasound system (23 MHz probe, Vinno Corporation, Suzhou, China). Mice were anesthetized with 1.5% isoflurane in a 95% oxygen/5% CO_2 mixture, and thoracic hair was removed the day prior. M-mode images were acquired from parasternal short-axis views, and left ventricular ejection fraction (EF) and fractional shortening (FS) were calculated.

Histological analysis

After echocardiography, mice were sacrificed, and heart tissues were collected, with portions stored at −80 °C. A subset was fixed in 4% paraformaldehyde, then transferred to 10% neutral-buffered formalin for 48 h at room temperature. Tissues were paraffin-embedded, sectioned at 5 μm, and stained with hematoxylin and eosin (H&E) to evaluate cardiac morphology under a light microscope (Motic, China).

TUNEL Assay

Myocardial apoptosis was assessed using the TUNEL kit (KGA704; KGI Biotechnology, Nanjing, China) according to the manufacturer's instructions. Nuclei were counterstained with DAPI, and apoptotic cells exhibited red fluorescence. Six high-power fields per sample were analyzed to calculate the apoptotic index (AI = apoptotic cells/total nucleated cells × 100%).

Quantitative Real-Time PCR (qRT-PCR)

Total RNA from tissues and cells was extracted using a Total RNA Extraction Kit (Foregene, China), followed by cDNA synthesis using RT Easy II (with gDNase) kit (Foregene, China). qRT-PCR was performed using SYBR Green I Master Mix (Foregene, China) on a LightCycler 96 instrument (Roche, Germany). GAPDH was used as the internal control, and relative gene expression was calculated using the $2^{-}\Delta\Delta Ct$ method. Primer sequences were as follows:

- PI3K: F 5'-CCGGAGGATGAAGCCACGCA-3'; R 5'-CAGGGCCGTTTCCGGTGTCT-3'
- AKT: F 5'-TAACGGACTCGGGCTGT-3'; R 5'-TTCTCGTGGTCCTGGTTGT-3'
- Bcl-xL: F 5'-TCTTCTCCTTTGGCGGGGCA-3'; R 5'-CAAGGGGCGGACACACAAGG-3'
- BCL-2: F 5'-GCCTCTACGGCCCCTTGTCG-3'; R 5'-CTCGCGGTGAAGGGCGTCAG-3'
- GAPDH: F 5'-ACTCTTCCACCTTCGATGCC-3'; R 5'-TGGGATAGGGCCTCTCTTGC-3'

Western blot analysis

Heart samples were homogenized in lysis buffer (Biyuntian Biotech, China) and centrifuged at 12,000 rpm for 10 minutes at 4℃ to obtain the protein-containing supernatant. Protein concentrations were determined using the BCA assay kit (Biyuntian Biotech). Equal amounts of protein were separated on 10% SDS-PAGE gels and transferred onto PVDF membranes. Membranes were blocked with 5% BSA in TBST (1× Tris-buffered saline with 0.1% Tween-20) for 1 hour at room temperature, then incubated overnight at 4℃ with primary antibodies. After washing three times with TBST, membranes were incubated with HRP-conjugated secondary antibodies for 1 hour at room temperature. Chemiluminescent signals were detected using an ECL substrate kit (Biosharp Life Science, China) and visualized on X-ray films. Band intensities were quantified using ImageJ (NIH, USA). Primary antibodies used included PI3K p85 alpha (60225-1-Ig), AKT (10176-2-AP), BCL2 (12789-1-AP), Bcl-XL (26967-1-AP), phospho-AKT Ser473 (28731-1-AP) from Proteintech (Wuhan, China), as well as anti-PI3K p85 alpha (phospho Y607, ab182651) and GAPDH (EPR16891) from Abcam (Shanghai, China).

Statistical analysis

Data are expressed as mean ± SD. For datasets following a normal distribution and equal variance, group comparisons were performed using one-way ANOVA, while paired t-tests were used for pre- and post-treatment comparisons. Non-parametric data were analyzed using the Kruskal-Wallis or Wilcoxon rank tests. Differences were considered statistically significant at $p < 0.05$. All statistical analyses were performed with SPSS 22.0 (IBM, USA).

Identification of active compounds in medicated rat serum by UPLC-Q-Exactive-Orbitrap-MS

To investigate the active components of ZGJTSXF, rats were administered the formula, and serum samples were collected for UPLC-Q-Exactive-Orbitrap-MS analysis. The total ion chromatograms revealed distinct chemical profiles in medicated serum compared to controls, representing potential bioactive compounds absorbed into the bloodstream **(Figure 2).** A total of 78 compounds were identified **(Table 1)** and categorized into flavonoids, small peptides, nucleosides, organic acids, phenylpropanoids, alkaloids, phenanthrenequinones, iridoids, phenols, and saponins. These compounds were considered the key active constituents of ZGJTSXF and were selected for subsequent target prediction and network pharmacology analysis.

Table 1. Identification of Blood-Entry components from ZGJTSXF in serum of rats

No.	Retention Time (min)	Precursor Ion (m/z)	Molecular Formula	Compound Name	Key Fragment Ions (m/z)	Chemical Class	Plant Source(s)
1	0.931	175.11911	$C_6H_{14}N_4O_2$	DL-Arginine	70.06522, 175.11899, 60.05593, 116.07062, 130.09756	Small peptides	Astragalus membranaceus
2	0.959	244.09302	$C_9H_{13}N_3O_5$	Cytidine	112.05056, 95.02399, 69.04485, 94.04008, 68.34165	Nucleosides	Rehmannia glutinosa
3	1.074	330.05869	$C_{10}H_{12}N_5O_6P$	Adenosine 3′,5′-cyclic monophosphate (cAMP)	136.06184, 330.05981, 98.98419, 69.03362, 119.03532	Nucleosides	Rehmannia glutinosa
4	1.096	344.04007	$C_{10}H_{12}N_5O_7P$	Guanosine 3′,5′-cyclic monophosphate (cGMP)	150.04204, 133.01555, 344.04007, 108.02032, 107.03622	Nucleosides	Rehmannia glutinosa

5	1.101	191.01984	$C_6H_8O_7$	Citric acid	111.00878, 87.00878, 85.02955, 191.01991, 129.01939	Organic acids	Crataegus pinnatifida / Panax ginseng
6	1.120	113.03468	$C_4H_4N_2O_2$	Uracil	113.03469, 70.02885, 96.00801, 113.02348, 113.0598	Nucleosides	Rehmannia glutinosa
7	1.126	173.00916	$C_6H_6O_6$	trans-Aconitic acid	85.0295, 129.01935, 111.00871, 173.00954, 86.03286	Organic acids	Cornus officinalis
8	1.139	190.07121	$C_7H_{11}NO_5$	N-Acetyl-L-glutamic acid	130.04996, 84.04443, 102.05501, 148.06041, 61.03994	Small peptides	Not specified
9	1.232	247.12917	$C_{10}H_{18}N_2O_5$	L-Isoleucyl-L-aspartic acid	86.09642, 69.06999, 247.12881, 72.08086, 56.04981	Small peptides	Not specified
10	1.243	117.01933	$C_4H_6O_4$	Succinic acid	73.02949, 117.0193, 99.00874, 74.03288, 118.0227	Organic acids	Panax ginseng / Rehmannia glutinosa / Crataegus pinnatifida
11	1.443	169.01428	$C_7H_6O_5$	Gallic acid	125.02444, 169.01434, 69.03465, 97.02953, 81.03461	Organic acids	Cornus officinalis
12	1.592	298.11487	$C_{11}H_{15}N_5O_5$	7-Methylguanosine	166.07243, 149.04585, 167.05634, 153.04074, 298.1373	Nucleosides	Rehmannia glutinosa
13	1.750	282.11987	$C_{11}H_{15}N_5O_4$	2′-O-Methyladenosine	136.06183, 282.11948, 119.03525, 69.03362, 137.04579	Nucleosides	Rehmannia glutinosa
14	1.758	361.11414	$C_{15}H_{22}O_{10}$	Catalpol	169.01424, 125.02438, 271.0462, 361.07776, 59.01383	Iridoid glycosides	Rehmannia glutinosa
15	1.974	298.11487	$C_{11}H_{15}N_5O_5$	2′-O-Methylguanosine	152.05681, 153.04082, 135.03024, 101.05983, 110.035	Nucleosides	Rehmannia glutinosa

16	2.277	731.22583	$C_{27}H_{42}O_{20}$	Rehmannioside D	179.05615, 263.07733, 71.01385, 59.01382, 89.02444	Iridoid glycosides	Rehmannia glutinosa
17	2.356	166.08641	$C_9H_{11}NO_2$	L-Phenylalanine	120.0808, 103.05421, 166.08623, 93.0699, 131.04916	Small peptides	Not specified
18	4.095	312.13034	$C_{12}H_{17}N_5O_5$	N^2,N^2-Dimethylguanosine	180.08795, 110.03492, 153.04073, 84.04442, 69.03363	Nucleosides	Rehmannia glutinosa
19	4.209	113.05981	$C_6H_8O_2$	Sorbic acid	113.05974, 67.0544, 95.04918, 71.04924, 85.06485	Organic acids	Crataegus pinnatifida
20	5.077	158.08224	$C_7H_{14}NO_3$	N-Acetyl-DL-norvaline	116.0717, 158.08226, 114.09244, 159.02986, 73.02948	Small peptides	Not specified
21		298.09698	$C_{11}H_{15}N_5O_3S$	5′-S-Methyl-5′-thioadenosine	136.06181, 298.09689, 61.01092, 75.02634, 119.03523	Nucleosides	Rehmannia glutinosa
5.334	299.11374	$C_{14}H_{20}O_7$	Salidroside	59.01384, 71.01385, 89.02445, 119.05005, 119.03504	Phenolic glycosides	Astragalus membranaceus	
23	5.633	229.15492	$C_{11}H_{20}N_2O_3$	Leucylproline	116.07057, 86.09637, 70.06519, 229.15466, 68.88325	Small peptides	Not specified
24	5.715	261.14462	$C_{11}H_{20}N_2O_5$	Glutamyl-Isoleucine	84.04442, 86.09641, 132.10196, 261.14468, 198.11235	Small peptides	Not specified
25	6.015	337.09302	$C_{16}H_{16}H_{18}O_8$	3-O-p-Coumaroylquinic acid	163.0401, 119.0502, 191.05614, 337.09348, 173.04591	Phenylpropanoids	Crataegus pinnatifida Bge
26	6.470	405.14008	$C_{18}H_{26}O_{11}$	Morroniside	101.02437, 155.03502, 141.05577, 243.08743, 179.0562	Iridoid glycosides	Cornus officinalis Sieb

27	6.689	433.11285	$C_{21}H_{20}O_{10}$	Puerarin xyloside	433.11295, 313.07065, 283.06009, 415.10242, 255.06516	Flavonoid glycosides	Pueraria lobata
28	7.490	263.13931	$C_{14}H_{18}N_2O_3$	Phenylalanyl-proline	120.08077, 116.07059, 70.06522, 263.13895, 103.05418	Small peptides	Not specified
29	7.637	417.11777	$C_{21}H_{20}O_9$	Puerarin	417.11801, 297.07574, 267.06512, 239.07022, 399.10742	Isoflavone glycosides	Pueraria lobata
30	7.741	291.08630	$C_{15}H_{14}O_6$	(+)-Catechin	139.039, 123.04406, 147.04404, 165.05464, 291.08691	Flavonoids	Astragalus membranaceus
31	7.839	172.09808	$C_8H_{15}NO_3$	N-Acetyl-D-allo-isoleucine	130.08727, 172.09793, 93.03456, 128.10809, 131.09084	Small peptides	Not specified
32 4-O-p-Coumaroylquinic acid	337.09302	$C_{16}H_{18}O_8$	173.0455, 93.03454, 163.04004, 119.05011, 337.09344	Phenylpropanoids	Crataegus pinnatifida Bge		
33	7.956	449.10788	$C_{21}H_{20}O_{11}$	Orientin	449.1077, 299.05484, 329.10714, 431.09714, 283.06006	Flavonoids	Salvia miltiorrhiza Bge
34	8.041	359.13345	$C_{18}H_{22}O_6$	Sweroside	197.08084, 127.03897, 179.07016, 111.08046, 95.04912	Iridoid glycosides	Cornus officinalis Sieb
35	8.075	447.12839	$C_{22}H_{22}O_{18}$	3'-Methoxypuerarin	447.12863, 327.0863, 297.07581, 429.11816, 134.03622	Flavonoid glycosides	Pueraria lobata
36	8.130	549.15985	$C_{26}H_{28}O_{16}$	Puerarin apioside	297.07578, 417.11804, 267.06516, 239.11804, 549.16022, 549.16022	Flavonoid glycosides	Pueraria lobata

37	8.144	342.16986	$C_{20}H_{23}NO_4$	(+)-Magnoflorine	342.17007, 58.06546, 297.11212, 265.08594, 282.08862	Alkaloids	Coptis chinensis Franch
38	8.236	211.14403	$C_{11}H_{18}N_2O_2$	Cyclo(Pro-Leu)	211.14412, 86.09641, 70.06522, 136.07574, 98.06007	Small peptides	Not specified
39	8.320	174.11270	$C_8H_{18}NO_3$	N-Acetyl-L-leucine	86.09642, 132.10196, 128.10703, 174.07648, 128.07059	Small peptides	Not specified
40	8.434	369.11832	$C_{16}H_{22}O_9$	3-O-Feruloylquinic acid	177.05463, 145.02843, 117.03352, 89.03857, 149.05978	Phenylpropanoids	Salvia miltiorrhiza Bge
41	8.561	4-O-Feruloyl-D-quinic acid	367.10330	$C_{17}H_{23}O_9$	173.0455, 93.03452, 134.03734, 193.05067, 137.02432	Phenylpropanoids	Salvia miltiorrhiza Bunge
42	8.745	211.14403	$C_{11}H_{18}N_2O_2$	Cyclo(Leu-Pro)	211.1441, 70.06524, 86.09643, 98.06008, 114.09142	Small peptides	Not specified
43	8.767	417.11777	$C_{21}H_{20}O_9$	Daidzin	255.06526, 199.07542, 137.02344, 181.06476, 91.05426	Isoflavone glycosides	Pueraria lobata
44	9.262	447.12839	$C_{22}H_{22}O_{10}$	Glycitin	285.07578, 270.05237, 253.04944, 213.05446, 137.02332	Flavonoid glycosides	Cornus officinalis Sieb
45	9.275	431.09836	$C_{21}H_{20}O_{10}$	Vitexin	311.0564, 431.09839, 283.06122, 133.02931, 135.04515	Flavonoids	Crataegus pinnatifida Bge
46	9.294	208.09691	$C_{11}H_{13}NO_8H_{13}NO_3$	N-Acetyl-L-Phenylalanine	120.08078, 166.0862, 162.09125, 208.09569, 103.05431	Small peptides	Not specified

47	9.566	300.99893	$C_{14}H_6O_8$	Ellagic acid	300.99905, 283.99643, 229.01419, 299.99142, 185.02452, 185.02452, 185.02452, 185.02452, 185.02452, 185.02452	Phenolic	Salvia miltiorrhiza Bunge
48	9.587	417.11777	$C_{21}H_{20}O_9$	Daidzein-6-C-glucoside	417.1178, 297.07562, 267.06506, 399.10727, 239.07013, 239.07013, 239.07013, 239.07013, 239.07013, 239.07013	Flavonoids	Pueraria lobata
49	9.729	417.11777	$C_{21}H_{20}O_9$	Daidzein 4′-O-glucoside	255.06503, 417.11786, 199.07524, 85.02837, 137.02332	Flavonoids	Pueraria lobata
50	9.864	447.12839	$C_{22}H_{22}O_{10}$	Calycosin-7-O-β-D-glucoside	285.07578, 270.05219, 137.02328, 213.05438, 225.05461	Flavonoids	Astragalus membranaceus
51	10.052	417.11777	$C_{21}H_{21}O_9$	Daidzein-5-C-glucoside	417.11823, 297.11823, 267.06522, 239.06522, 399.10757, 399.10757	Flavonoid glycosides	Pueraria lobata
52	10.064	257.08078	$C_{15}H_{12}O_4$	Liquiritigenin	137.02333, 147.04399, 81.03351, 119.04916	Flavonoids	Pueraria lobata
53	11.175	283.06122	$C_{16}H_{12}O_5$	Biochanin A	283.06134, 268.03787, 211.04012, 239.03543, 240.04276	Flavonoids	Crataegus pinnatifida Bge
54	11.429	336.12277	$C_{20}H_{13}N_6O_3$	Epiberberine	336.12283, 320.09164, 292.09665, 262.08618, 290.08102, 290.08102	Alkaloids	Coptis chinensis Franch.

55	11.558	338.13852	$C_{23}H_{16}O_6$	Dihydroberberine	338.13855, 322.1073, 279.08902, 294.11218, 265.07349	Alkaloids	Coptis chinensis Franch
56	11.803	338.13852	$C_{23}H_{1}$◆BC	Jatrorrhizine	338.13855, 322.10736, 279.08896, 294.11224, 265.07336	Alkaloids	Coptis chinensis Franch
57	11.866	359.07739	$C_{18}H_{16}O_8$	Rosmarinic acid	161.02443, 197.04559, 135.04517, 72.9931, 133.02951, 133.02951, 133.02951	Phenylpropanoids	Salvia miltiorrhiza Bunge
58	12.160	537.10394	C_{24}.10394	Lithospermic acid	295.06131, 109.0294, 185.02446, 135.0451, 135.0451, 135.0451, 135.0451	Phenylpropanoids	Salvia miltiorrhiza Bunge
59	12.709	717.14648	C_{33333}.05112, 339.05112, 339.051, 295.06131, 339.051, 339.051, 339.051	Salvianolic acid B	321.04053, 519.09344, 109.0451, 339.051, 295.065, 109.02946, 339.02946, 339.051, 295.06131	Phenylpropanoids	Salvia miltiorrhiza Bunge
60	12.880	255.06524	$C_{15}H_{10}O_4$	Daidzein	255.06509, 199.0753, 137.02332, 91.0542, 227.07022	Flavonoids	Pueraria lobata
61	12.981	159.10268	C_3-Hydroxyoctanoic acid	59.01382, 159.0298, 73.02939, 129.01939, 129. Organic acids	$C_6H_{16}O_6$Luteolin	Flavonoids	Astragalus membran Luteolin
63	13.083	257.08090	$C_{16}H_{12}O_4$	Isoliquiritigenin	257.08099, 137.02338, 147.04405, 81.03354, 91.05424	Flavonoids	Pueraria lobata
64	13.339	285.07596	$C_{16}H_{12}O_5$	Glycitein	285.07565, 270.05225, 137.0233, 213.05452, 253.04939	Flavonoids	Pueraria lobata

65	13.569	336.12277	$C_{20}H_{16}O_5$	Berberine	336.12311, 320.09192, 292.09692, 278.08133, 318.07626	Alkaloids	Coptis chinensis Franch
66	13.580	493.11417	$C_{26}H_{22}O_{10}$	Salvianolic acid A	295.0611, 109.0294, 185.02438, 135.0451, 159.04507	Phenylpropanox	Salvia miltiorrhizina Bunge
67	13..678	463.16034	$C_{23}H_{26}O_{16}$	Methylnissolin-3-O-glucoside	167.07025, 301.10709, 152.0468	Phenolic glycosides	106.041, 463.16034
68	13.688	201.11340	$C_{18}H_{18}O_6$	Sebacic acid	111.02, 202.11624, 139.1129, 183.10269, 111.02, 202.11624	Organic acids	Cornus officinalis Sieb
69	13.759	285.07596	$C_{16}H_{12}O_6$	Calycosin	285.07568, 270.05222, 253.		
70	15.102	269.04559.045, 63.02398, 224.04774, 181.06627	Flavonoids	Genistein	269.045, 133.02943, 63.02398, 224.045, 181.	Flavonoids	Pueraria lobata
71	17.279	269.08072	$C_{16}H_{12}O_4$	Formononetin	269.08075, 197.05965, 253.04947, 237.05455, 269.08075, 237.05455, 254.05742, 269.05742	Flavonoids	Pueraria lobata
71	18.803	991.54892	$C_{48}H_{82}O_{18}$	Ginsenoside Re	71.01385, 101.440, 783.48871.440, 621.440, 459.38547, 459.38547, 783.48871, 621.440, 459.38547, 71.01385, 101.02438, 783.545.385, 621.440, 459.38547, 459.385, 459.385, 459.385, 459.385,	Saponins	

72	18.803	991.54892	$C_{48}H_{82}O_{18}$	Ginsenoside Re	71.01385, 101.02438, 783.48871, 621.44098, 459.38547, 783.48871, 621.440, 459.385, 459.385, 459.385	Saponins	
73	20.255	283.06122	C_{18}	Texasin	283.06128, 268.03787, 267.03006, 239.03503, 211.04021	Flavonoids	
	22.545	279.10162	$C_{18}H_{14}O_8$	Dihydrotanshinone I	279.10175, 233.09631, 205.10136, 190.07774, 261.09125, 261.09631, 190.07774, 261.09631, 261.	Phenanthrenequinones	Salvia miltiorrhiza Bunge
75	24.250	297.14853	$C_{18}H_{15}O_3$	Cryptotanshinone	297.14862, 251.14304, 254.09386, 282.12518, 279.12518, 279.13794, 297.14862, 251.14304, 254.09386, 282.12518, 279.13794	Phenanthrenequinones	Salvia miltiorrhiza Bunge
76	24.874	279.10178	$C_{18}H_3$	Dihydroisotanshinone II	261.09116, 190.07771, 233.09622, 205.10127, 189.06987, 261.09116, 190.07771, 233.09622, 205.	Phenanthrenequinones	Salvia milt
77	25.112	295.22690	$C_{18}H_{30}O_3$	9-O-(10E, 9-O-(10E), 277.21631, 81.03353, 67.0544, 81.06989, 79.05424, 277.05424, 81.054, 81.054, 81.054,	Organic acids	Crataegus pinnatifida Bge	

78	25.648	295.13300	$C_{18}H_{18}O_3$	Tanshinone IIA	295.13315, 249.1275, 277.12247, 191.08549, 206.10921, 277.12247, 191.08549, 206.10921	Phenanthrenequinone	Salvia miltiorrhiza Bunge

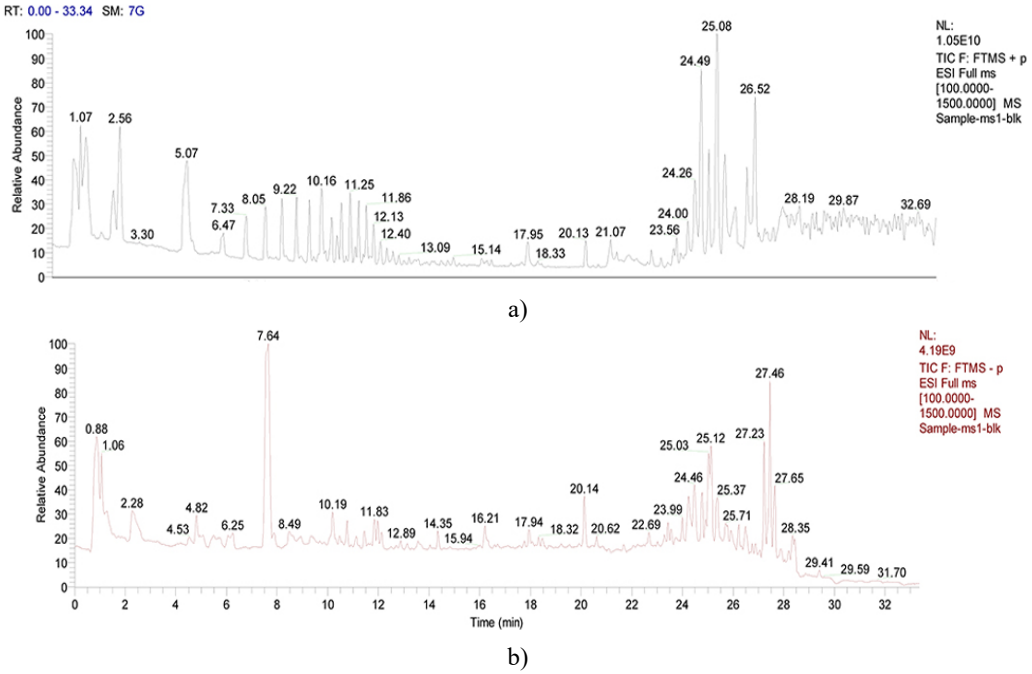

Figure 2. Total ion chromatography of the blood-entry compounds of ZGJTSXF in the positive and negative ion mode by UHPLC-Q-Orbitrap-MS.

Total ion chromatography and network analysis of ZGJTSXF blood-entry compounds

The total ion chromatograms of ZGJTSXF blood-absorbed components were acquired in both positive and negative ion modes using UHPLC-Q-Orbitrap-MS **(Figure 2).** To explore the molecular targets of these compounds, we analyzed the 78 identified serum-absorbed constituents using multiple databases. The SMILES strings for each compound were submitted to the PubChem database and analyzed with Swiss Target Prediction, which yielded 827 predicted protein targets (note: one compound lacked a SMILES entry and five compounds had no predicted targets).

In parallel, 1,357 candidate targets associated with diabetic cardiomyopathy (DCM) were collected by querying the DisGeNET, NCBI-gene, and GeneCards databases. By intersecting the predicted compound targets with DCM-associated targets, 228 overlapping proteins were identified as potential mediators of ZGJTSXF's therapeutic effects in DCM. These 228 targets, together with the 78 blood-entry compounds, were used to construct a compound-target interaction network. The resulting network consisted of 319 nodes and 1,491 edges, visually illustrating the complex interactions between ZGJTSXF components and their putative targets **(Figure 3).**

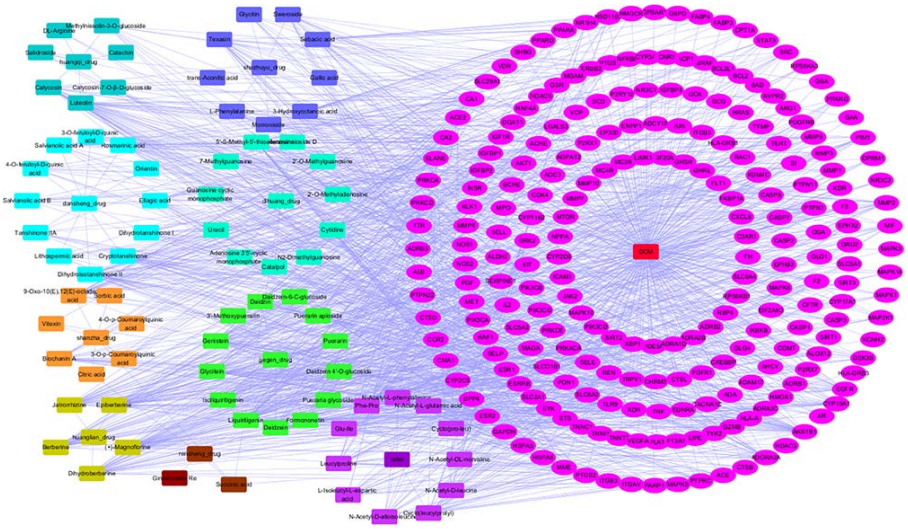

Figure 3. The component-target network of ZGJTSXF in the treatment of DCM.

Protein-Protein Interaction (PPI) network analysis of ZGJTSXF targets

The 228 shared targets were uploaded to the STRING database to construct a protein-protein interaction (PPI) network. Targets lacking any interactions were removed from the analysis. The resulting PPI data were imported into Cytoscape for visualization, where nodes represented individual target proteins and edges indicated interactions between them. Edge color and thickness corresponded to the combined interaction score, and nodes were arranged in six concentric circles according to their degree values **(Figure 4).**

In this network, the average node degree was calculated as 32. Proteins with a degree value exceeding twice the average were defined as core targets. Using this criterion, 29 key proteins were identified, including ALB, TNF, AKT1, GAPDH, VEGFA, EGFR, SRC, CASP3, MAPK3, JUN, PPARG, STAT3, ESR1, MMP9, HRAS, ERBB2, CXCL8, MTOR, PTGS2, SIRT1, PPARA, MAPK1, ACE, BCL2L1, IL2, MMP2, ICAM1, PTPRC, and NFKBIA. These core targets were considered the most relevant mediators for ZGJTSXF in treating DCM.

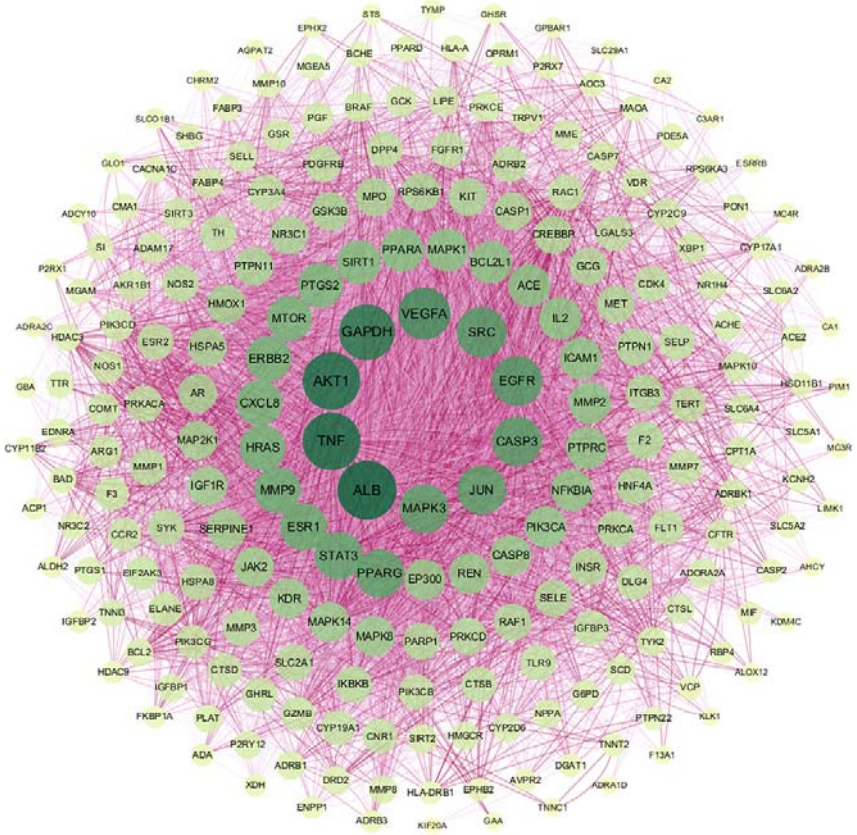

Figure 4. The PPI network was constructed using the common targets to predict core target proteins of ZGJTSXF. The color and thickness of the configuration edge follow the combine_score to continuously change, and finally the target genes were laid out into six concentric circles according to the node degree. The degree of the target gene node is between 21–32; the degree of the node in the fourth layer is between 33 and 40; the degree of the node in the third layer is between 41 and 60; the degree of the node in the second layer is between 60 and 100; and the degree of the node in the innermost layer is between 33 and 40. The larger the value of the parameter Degree in the figure, the larger the shape of the corresponding node and the darker the color.

PPI network construction and core target identification

A protein-protein interaction (PPI) network was generated using the shared targets to identify key proteins potentially regulated by ZGJTSXF **(Figure 4).** In the network, nodes represented target genes, and edges represented interactions, with edge color and thickness corresponding to the combined interaction score. Nodes were organized into six concentric layers based on their degree values: nodes in the outermost layer had degrees of 21–32, the fourth layer 33–40, the third layer 41–60, the second layer 60–100, and the innermost layer 33–40. Node size and color intensity increased with higher degree values, highlighting the most connected and potentially influential targets.

Gene Ontology (GO) and KEGG pathway enrichment analysis

GO enrichment analysis was performed to investigate the biological roles, cellular localization, and molecular functions of the identified targets. A total of 2,845 GO terms were significantly enriched, including 2,550 biological processes (BP), 181 molecular functions (MF), and 114 cellular components (CC). Analysis of biological processes indicated involvement in nutrient response, protein secretion, and protein localization to the extracellular region. For cellular components, targets were mainly enriched in membrane rafts, membrane microdomains, general membrane regions, and glutamatergic synapses. Molecular function enrichment highlighted activities such as endopeptidase activity, protein serine/threonine kinase activity, and protein tyrosine kinase activity **(Figure 5a).**

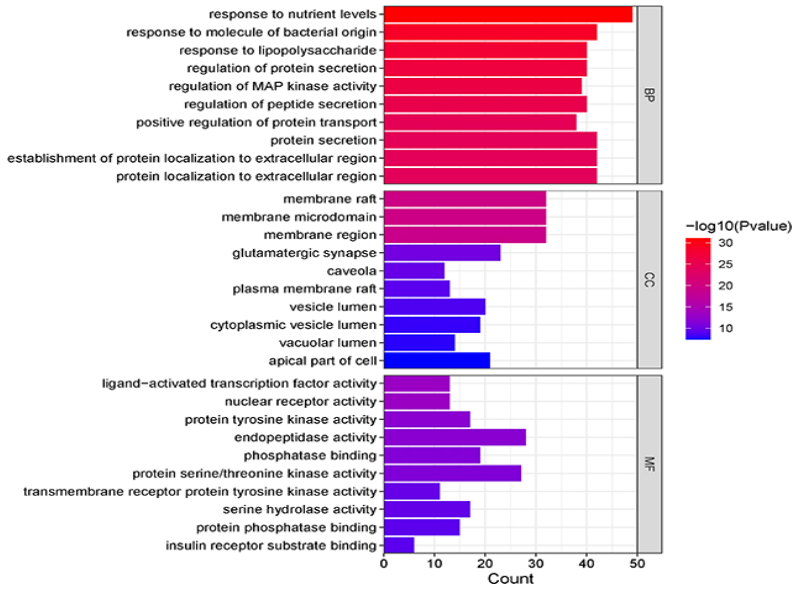

a)

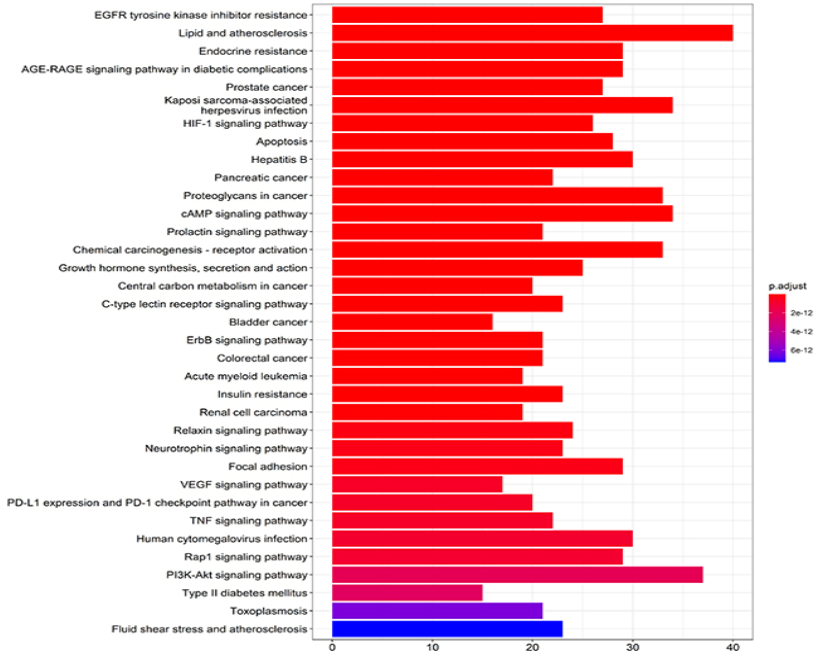

b)

Figure 5. GO enrichment and KEGG pathway analysis identified critical pathways associated with ZGJTSXF. (a) The top 10 enrichment items of Biological Process, Molecular Function and Cellular Components from GO enrichment analysis. (b) The top 35 pathways of KEGG pathway analysis.

GO and KEGG pathway analysis highlighted key biological pathways of ZGJTSXF

GO enrichment and KEGG pathway analyses were performed to elucidate the biological processes and signaling pathways potentially regulated by ZGJTSXF **(Figure 5).** In GO enrichment, the top 10 terms were identified for biological processes, molecular functions, and cellular components **(Figure 5a).**

KEGG pathway enrichment analysis, commonly used to investigate functions and signaling networks of differentially expressed genes, revealed 185 pathways [16]. The most significantly enriched pathways included lipid and atherosclerosis, PI3K-AKT signaling, cAMP signaling, Kaposi's sarcoma-associated herpesvirus

infection, hepatitis B, and apoptosis. The top 35 pathways, ranked by P value, were visualized in a pathway diagram **(Figure 5b),** emphasizing the critical roles of the PI3K/AKT signaling and apoptosis pathways in ZGJTSXF's action.

ZGJTSXF reduced fasting blood glucose and improved glucose tolerance in DCM mice

To experimentally validate the predictions from the in silico network pharmacology analysis, the therapeutic effects of ZGJTSXF were evaluated in a DCM mouse model. Fasting blood glucose (FBG) levels were first assessed. As expected, FBG levels in the DCM model group were significantly elevated compared with the control group (P<0.01). After four weeks of treatment, mice in the metformin group and all ZGJTSXF-treated groups exhibited significantly lower FBG levels than the untreated DCM group (P<0.01). Among the ZGJTSXF-treated groups, the medium-dose group (ZGJTSXFM) showed the greatest reduction in FBG compared with the low- and high-dose groups, with the difference reaching statistical significance (P<0.01) **(Table 2)**. These results confirm that ZGJTSXF effectively lowers FBG in DCM mice.

Table 2. Fasting blood glucose levels before and after treatment in all groups of mice

Group	Time	FBG (mmol/L)
CON	Before treatment	4.33±0.142
	After treatment	4.42±0.255
DCM	Before treatment	16.11±0.599$^{\#\#}$
	After treatment	16.20±0.799$^{\#\#}$
Met	Before treatment	16.09±0.396
	After treatment	9.56±0.257$^{▲▲}$
ZGJTSXFL	Before treatment	16.09±0.629
	After treatment	12.95±0.761$^{▲▲}$
ZGJTSXFM	Before treatment	16.16±0.199
	After treatment	9.58±0.292$^{▲▲**ΔΔ}$
ZGJTSXFH	Before treatment	15.77±0.566
	After treatment	13.02±0.258$^{▲▲}$

Notes: $^{\#\#}P$<0.01, compared with the CON group; $^{▲▲}P$<0.01, compared with the DCM group; $^{**}P$<0.01, compared with the ZGJTSXFL group; ^{ΔΔ}P<0.01, compared with the ZGJTSXFH group.

We next assessed the effects of ZGJTSXF on oral glucose tolerance in DCM mice. As shown in **Table 3**, following glucose administration, blood glucose levels in the DCM group were significantly higher at all time points compared with the control group (P<0.01). Treatment with metformin and the medium-dose ZGJTSXF group (ZGJTSXFM) markedly reduced the glucose increase in DCM mice (P<0.01). The low-dose (ZGJTSXFL) and high-dose (ZGJTSXFH) groups also significantly attenuated the blood glucose rise at the 60-minute mark (P<0.01). All treatment groups showed a significant reduction in the area under the curve (AUC) compared with the DCM group (P<0.01). Among the ZGJTSXF-treated groups, the medium-dose group demonstrated the strongest improvement in oral glucose tolerance, with a statistically significant advantage over the low- and high-dose groups (P<0.01). Overall, these findings indicate that ZGJTSXF effectively enhances oral glucose tolerance in DCM mice.

Table 3. Oral glucose tolerance test results in all groups of mice

Group	0Min	30Min	60Min	120Min	AUC (mmol*h/L)
CON	4.36±0.285	11.92±1.555	7.25±1.455	5.44±0.458	15.21±0.858
DCM	16.65±0.83$^{\#\#}$	30.97±1.901$^{\#\#}$	30.65±1.853$^{\#\#}$	20.88±2.491$^{\#\#}$	53.08±2.133$^{\#\#}$
Met	9.64±0.256$^{▲▲}$	25.05±1.617$^{▲▲}$	16.66±1.941$^{▲▲}$	10.96±0.167$^{▲▲}$	32.91±1.531$^{▲▲}$
ZGJTSXFL	12.88±0.695	30.74±1.587	21.97±2.129$^{▲▲}$	14.02±0.241	42.08±2.185$^{▲▲}$
ZGJTSXFM	9.82±0.242$^{▲}$	26.31±1.754$^{▲▲**ΔΔ}$	17.72±2.549$^{▲▲**}$	11.03±0.216$^{▲}$	34.42±2.29$^{▲▲**ΔΔ}$

ZGJTSXFH	12.94±0.382	30.57±3.944	19.78±3.067▲▲	14.19±0.450	40.45±3.966▲▲

Notes: ##*P*<0.01, compared with the CON group;▲▲*P*<0.01,▲*P*<0.05, compared with the DCM group; **P<0.01, compared with the ZGJTSXFL group; ΔΔ*P*<0.01, compared with the ZGJTSXFH group.

ZGJTSXF Administration Enhanced Cardiac Function and Ameliorated Myocardial Histology in DCM Mice

We further investigated the effects of ZGJTSXF on cardiac function using echocardiography in DCM mice. As illustrated in **Figures 6a–6c**, mice in the DCM group exhibited significantly decreased left ventricular ejection fraction (LVEF) and left ventricular fractional shortening (LVFS) compared with the control group. Importantly, treatment with metformin and all doses of ZGJTSXF (low, medium, and high) significantly improved both LVEF **(Figure 6c)** and LVFS **(Figure 6c)** (P<0.01). Moreover, the medium-dose ZGJTSXF group (ZGJTSXFM) showed significantly greater improvements in LVEF and LVFS than both the low-dose (ZGJTSXFL) and high-dose (ZGJTSXFH) groups (P<0.01).

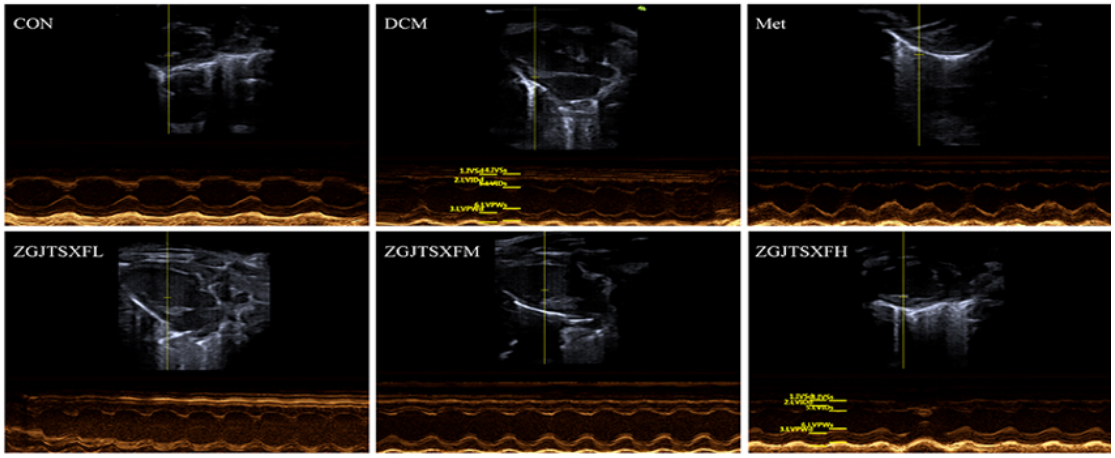

a)

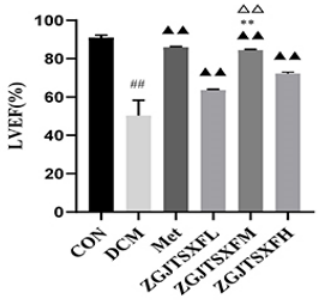

b)

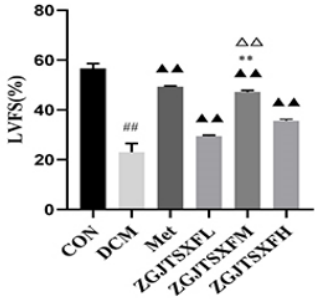

c)

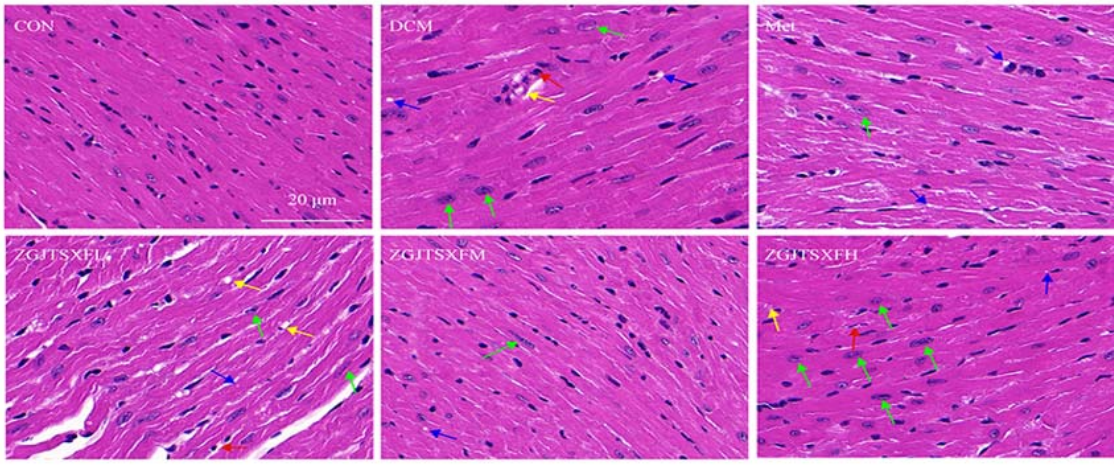

d)

Figure 6. Illustrates the effects of ZGJTSXF on cardiac function and myocardial histology in DCM mice. Panels a–c display echocardiographic assessments across different groups. (a) Representative M-mode echocardiograms. (b) Left ventricular fractional shortening (FS). (c) Left ventricular ejection fraction (EF). Statistical significance: ##P<0.01 versus CON; ▲▲P<0.01 versus DCM; **P<0.01 versus ZGJTSXFL; ΔΔP<0.01 versus ZGJTSXFH. (D) Histopathology of myocardial tissues by H&E staining (scale bar, 20 μm): (a) CON; (b) DCM; (c) Met; (d) ZGJTSXFL; (e) ZGJTSXFM; (f) ZGJTSXFH. Green arrow indicates cardiomyocyte hypertrophy, red arrow shows small focal inflammatory infiltration, blue arrow denotes vacuolar degeneration, and yellow arrow highlights capillary basement membrane thickening.

Histological analysis revealed that myocardial tissue in the CON group exhibited normal structure, with evenly sized nuclei, well-arranged ventricular wall and papillary muscle cells, and intact morphology without pathological alterations. In contrast, the DCM group displayed interstitial widening, cardiomyocyte hypertrophy (green arrow), inflammatory infiltration (red arrow), vacuolar degeneration (blue arrow), capillary basement membrane thickening (yellow arrow), and coagulative necrosis. Treatment with metformin or ZGJTSXF significantly alleviated these pathological changes, with the medium-dose ZGJTSXF group (ZGJTSXFM) showing the most pronounced improvement **(Figure 6d).** These findings indicate that ZGJTSXF administration enhances myocardial structure and function in DCM mice.

Next, we evaluated whether ZGJTSXF could modulate cardiomyocyte apoptosis and the PI3K-AKT signaling pathway. TUNEL staining demonstrated a markedly higher cardiomyocyte apoptosis rate in the DCM group compared to CON (P<0.01) **(Figures 7a and 7b).** Administration of metformin or ZGJTSXF at all doses significantly reduced apoptosis (P<0.01). Among the ZGJTSXF-treated groups, the medium-dose group (ZGJTSXFM) exhibited the lowest apoptosis rate (P<0.01 and P<0.05), although none of the ZGJTSXF groups surpassed the anti-apoptotic effect of metformin **(Figure 7b).**

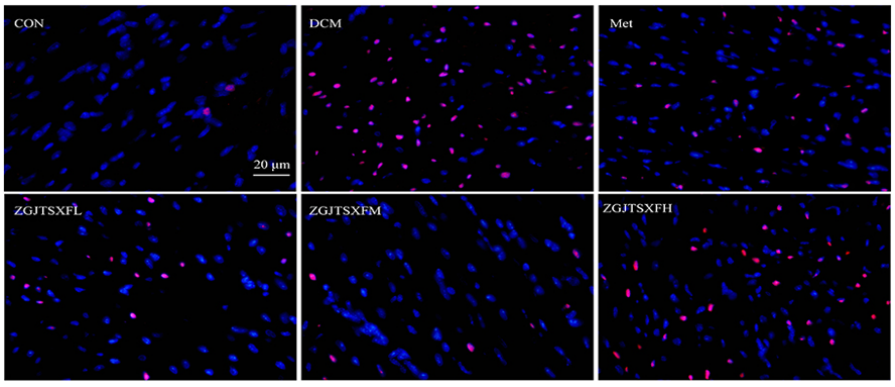

a)

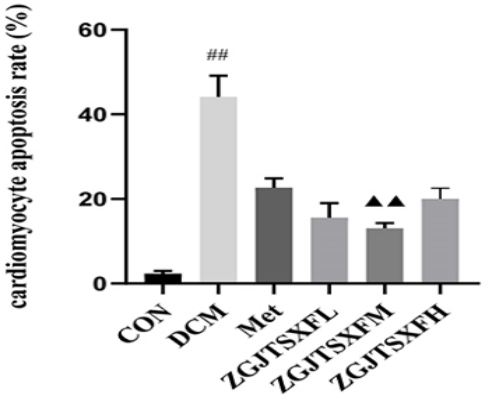

b)

Figure 7. shows TUNEL staining results evaluating apoptosis in mouse myocardial tissues. (a) Representative images of cardiomyocyte apoptosis (scale bar, 20 μm). (b) Quantification of the cardiomyocyte apoptosis rate for each group (n=6 per group). Statistical significance: ##P<0.01 versus CON; ▲▲P<0.01 versus DCM; **P<0.01, *P<0.05 versus ZGJTSXFM.

To validate the predicted effects of ZGJTSXF on the PI3K-AKT signaling and apoptosis pathways, mRNA and protein expression levels of PI3K, AKT, Bcl-2, and Bcl-xL were measured using qPCR and Western blotting **(Figure 8).** Compared with CON, DCM mice showed significantly lower mRNA levels of PI3K **(Figure 8a),** AKT **(Figure 8b),** Bcl-2 **(Figure 8c),** and Bcl-xL **(Figure 8d)** in myocardial tissues (P<0.01). Following 4 weeks of treatment, both the Met and ZGJTSXFM groups exhibited markedly increased mRNA levels of PI3K, AKT, Bcl-2, and Bcl-xL compared with the DCM group (P<0.01). In the ZGJTSXFH group, PI3K, AKT, and Bcl-xL expression levels were significantly elevated relative to DCM, though Bcl-xL showed no significant change.
Western blot results **(Figure 8e)** largely mirrored the mRNA findings. Both Met and ZGJTSXF treatments significantly restored the p-PI3K/PI3K **(Figure 8f)** and p-AKT/AKT **(Figure 8g)** ratios, which were suppressed in DCM mice (P<0.05). Protein levels of Bcl-2 (**Figure 8h)** and Bcl-xL **(Figure 8i)** were significantly higher in the Met and ZGJTSXFM groups compared with DCM (P<0.05). Among ZGJTSXF-treated groups, the medium-dose group (ZGJTSXFM) demonstrated the most pronounced increase in Bcl-2 and Bcl-xL expression, with statistical significance versus the low- and high-dose groups (P<0.01). Overall, these results indicate that ZGJTSXF mitigates cardiomyocyte apoptosis and activates the PI3K-AKT signaling pathway in DCM mouse myocardial tissues.

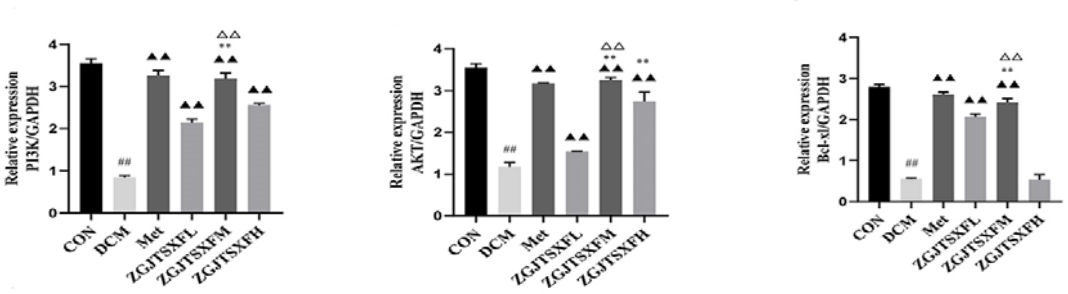

a) b) c)

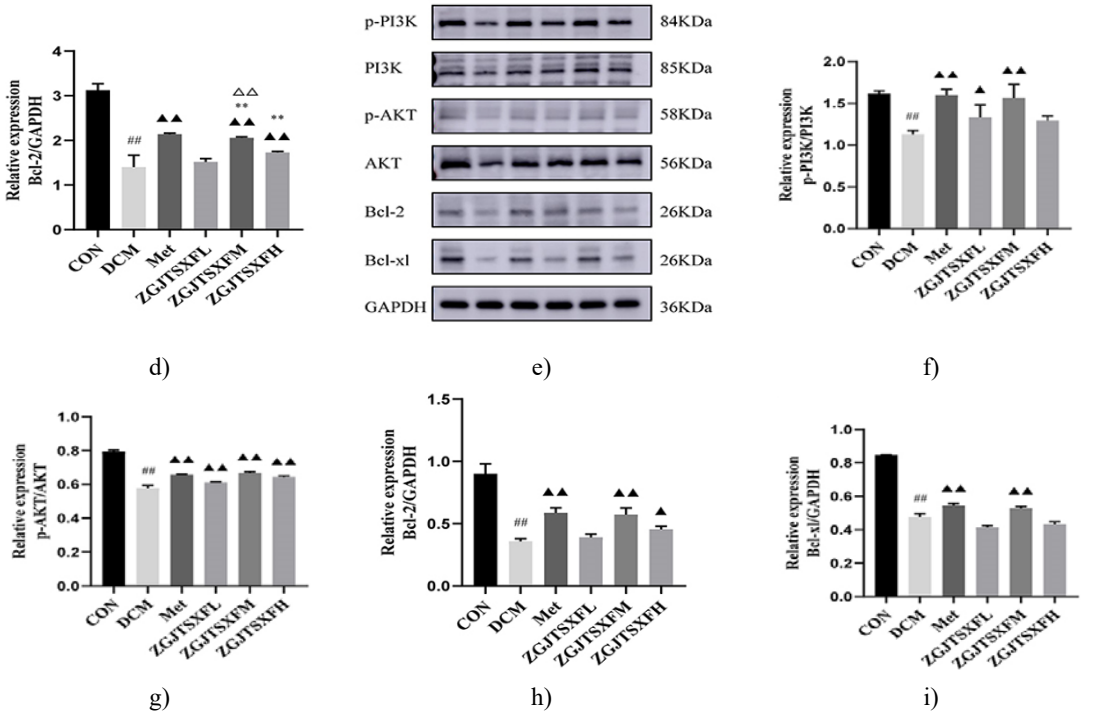

Figure 8. The expression levels of PI3K-AKT pathway molecules and apoptosis-related molecules in mouse myocardial tissues were quantitated. (a–d) The mRNA levels of PI3K (a), AKT (b), Bcl-2 (c), and Bcl-xL (d) in mouse myocardial tissues of the indicated groups were quantitated by qPCR. n=6 for each group; ##P<0.01, Compared with the CON group; ▲▲P<0.01, compared with the DCM group; **P<0.01, compared with the ZGJTSXFL group; ΔΔP<0.01, compared with the ZGJTSXFH group. (e–i) The protein levels of phosphorylated PI3K (p-PI3K; (f), phosphorylated AKT (p-AKT; (g), Bcl-2 (h), and Bcl-xL (i) in mouse myocardial tissues of the indicated groups were quantitated by Western blot assay. Representative images of Western blot bands are shown (e), and the relative expressions were summarized. n=6 for each group; ##P<0.01, compared with the CON group; n=6 for each group; ▲▲P<0.01, ▲P<0.05, compared with the DCM group.

Diabetic cardiomyopathy (DCM) is a major complication of diabetes mellitus and a leading cause of death in diabetic patients.1,4 Its development involves multiple proteins, pathways, and complex mechanisms, making single-target drugs insufficient for effective treatment.1,4 ZGJTSXF, with its multi-component and multi-target characteristics, has demonstrated promising therapeutic effects in DCM.9,10 In this study, we found that ZGJTSXF improved blood glucose levels and mitigated diabetic cardiomyocyte injury by inhibiting apoptosis, aligning with the holistic and synergistic principles of Traditional Chinese Medicine (TCM). However, conventional pharmacological approaches are insufficient to fully clarify the active components and mechanisms of ZGJTSXF. To address this, we applied an integrated approach combining serum pharmacochemistry and network pharmacology, followed by experimental validation, to systematically explore the compounds and mechanisms of ZGJTSXF in DCM. Our findings indicate that ZGJTSXF protects the myocardium in DCM by regulating the PI3K/Akt pathway and reducing cardiomyocyte apoptosis.

Through UPLC-Q-Exactive-Orbitrap-MS analysis of rat serum after ZGJTSXF administration, we identified 78 main active compounds. These compounds have been reported to exert beneficial effects in various diseases. Flavonoids, including puerarin, daidzin, luteolin, calycosin-7-O-β-D-glucoside, calycosin, and formononetin, were the most abundant and are known to alleviate DCM and other cardiovascular complications through anti-hyperglycemic [17] anti-hyperlipidemic, [18] antioxidant, [19] anti-inflammatory, [20] and anti-apoptotic [21] activities. Small peptides such as N-acetyl-D-leucine, Cyclo(leucylprolyl), and N-acetyl-L-phenylalanine can modulate biological activity, prevent oxidative stress, and reduce inflammation, thereby helping prevent diabetes [22]. Organic acids, including gallic acid and sorbic acid, possess antioxidant, antimicrobial, and anticancer properties, and gallic acid can reduce inflammation, oxidative stress, and diabetes-induced hypotension by

increasing plasma miR-24 and miR-126 levels [23]. Phenylpropanoids like rosmarinic acid, salvianolic acid A, and salvianolic acid B also exert protective effects in diabetic or obese animal models [24–27]. These findings highlight the multi-component nature of ZGJTSXF and support its advantage in regulating multiple targets and pathways.

Network pharmacology further identified multiple potential targets and signaling pathways for ZGJTSXF, with apoptosis and the PI3K-AKT pathway being particularly relevant. Cardiomyocyte apoptosis is a critical event in DCM pathogenesis, regulated by complex molecular mechanisms.1,5 Modulating apoptotic pathways can effectively reduce cardiomyocyte death. The PI3K/Akt signaling pathway plays a key role in cell survival, apoptosis, and proliferation. Activation of this pathway reduces cardiomyocyte apoptosis and myocardial injury, while its inhibition has the opposite effect [28–30]. Phosphorylation of upstream kinases, such as PDK1, triggers Akt activation, providing survival signals and counteracting apoptotic stimuli.32 This process involves the balance between pro-apoptotic and anti-apoptotic proteins [31].

The Bcl-2 family of proteins regulates apoptosis, including pro-apoptotic members (BAK, BAX, BAD) and anti-apoptotic members (Bcl-2, Bcl-xL) [32]. Increased apoptosis correlates with reduced expression of anti-apoptotic proteins Bcl-2 and Bcl-xL [33]. In our study, ZGJTSXF treatment upregulated Bcl-2 and Bcl-xL expression in myocardial tissues, indicating reduced apoptosis. Moreover, ZGJTSXF activated the PI3K/Akt signaling pathway, which was associated with increased levels of these anti-apoptotic proteins **(Figure 9).** These results are consistent with previous studie [28–30] and support a strong link between PI3K-AKT pathway activation and inhibition of cardiomyocyte apoptosis.

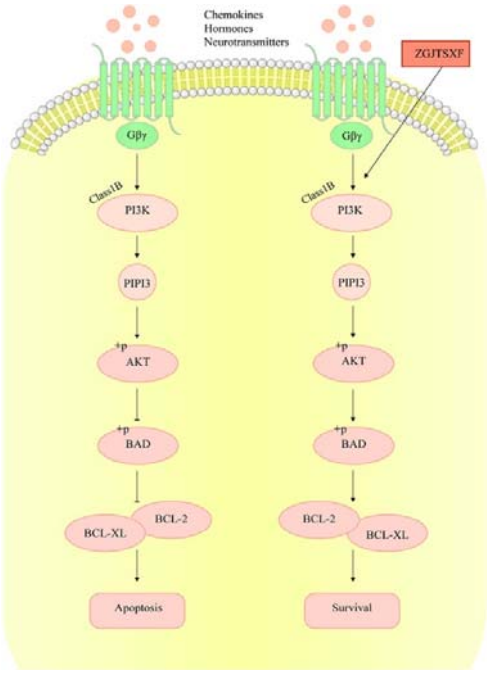

Figure 9. ZGJTSXF inhibits cardiomyocyte apoptosis by regulating PI3K/Akt signaling pathway

We employed spontaneous nonobese T2DM MKR mice fed a high-fat diet to establish the DCM model, as MKR mice are considered one of the most suitable animal models for investigating T2DM and its complications [34]. In this study, fasting plasma glucose levels in the model group were markedly elevated compared with the control group. Subsequent histological examination and echocardiographic assessments further confirmed that the DCM model was successfully created. Metformin, the positive control drug and a biguanide derivative, is known for its strong glucose-lowering activity and is widely recommended as a first-line therapy for type 2 diabetes mellitus [35]. Previous research demonstrated that metformin improves several clinical parameters and reduces cardiovascular events in Chinese patients with type 2 diabetes compared with lifestyle modification alone [36]. Additionally, Zhang *et al*. reported that metformin provides cardioprotective benefits by attenuating myocardial structural injury, inhibiting cardiomyocyte apoptosis, and suppressing inflammatory responses in both in vivo and in vitro settings [37]. Metformin can regulate the expression of multiple biomarkers and signaling cascades,

including AMPK, endothelial nitric oxide synthase (eNOS), NF-κB, and the PI3K/AKT pathways, thereby exerting anti-inflammatory, anti-apoptotic, and antioxidant effects [38].

In this investigation, we observed that both the Met and ZGJTSXF treatment groups alleviated cardiomyocyte hypertrophy, vacuolar degeneration, inflammatory cell infiltration in the myocardial interstitium, thickening of the capillary basement membrane, and myocardial fibrosis associated with diabetic cardiomyopathy, ultimately improving cardiac function. Based on predictions from network pharmacology analysis, we concentrated on the PI3K/AKT signaling pathway in exploring the mechanisms by which ZGJTSXF mitigates myocardial apoptosis in diabetic cardiomyopathy. Our findings revealed that ZGJTSXF activated the PI3K/AKT pathway and modulated the expression of Bcl-2 and Bcl-xL proteins in a manner comparable to metformin. Notably, the medium-dose ZGJTSXF group displayed better therapeutic efficacy across several parameters than the high-dose group, suggesting that excessive dosing may induce potential side effects.

This study has certain limitations. First, our investigation of ZGJTSXF's anti-apoptotic effects relied solely on mouse myocardial tissues. Given the difficulty of obtaining human cardiac samples, clinical trials have yet to begin, indicating that further efforts are needed to enhance the translational relevance of these findings. In future work, we aim to conduct randomized controlled clinical studies. Second, we did not assess the dynamic alterations in the PI3K/AKT and apoptosis pathways in cardiomyocytes of DCM mice following ZGJTSXF treatment. Moreover, since tissue samples were collected only after a 4-week intervention, both short-term and long-term effects of ZGJTSXF require more thorough investigation.

Conclusion

In this study, we elucidated the active constituents and molecular mechanisms of ZGJTSXF against DCM using an integrated approach that combined UPLC-Q-Exactive-Orbitrap analysis, network pharmacology, and experimental validation. A total of 78 components of ZGJTSXF were identified and incorporated into network pharmacological analysis. By experimentally confirming the hub targets and key signaling pathways predicted through network pharmacology, we demonstrated that ZGJTSXF exerts protective effects on diabetic cardiomyopathy by inhibiting cardiomyocyte apoptosis and restoring PI3K/AKT signaling in mouse myocardial tissue. These findings provide new insights into the development of ZGJTSXF-based therapeutics and support its potential clinical application in the treatment of DCM. Furthermore, our study highlights that integrating network pharmacology with experimental validation is a powerful strategy for clarifying the multi-target and multi-pathway mechanisms characteristic of traditional Chinese medicine formulas.

Acknowledgments: None

Conflict of Interest: None

Financial Support: This work was supported by grants from the National Natural Science Foundation of China (82074400), Hunan Provincial Technology Key Research and Development Program (2020SK2101), National Natural Science Foundation of China (82004185), National Natural Science Foundation of China (U21A20411), Postgraduate Research and Innovation Project of Hunan Province (CX20210692), and Hunan Provincial Key Laboratory of Translational Medicine for TCM Recipe and Syndrome Research (2018TP1021).

Ethics Statement: None

References

1. Jia G, Hill MA, Sowers JR. Diabetic cardiomyopathy: an update of mechanisms contributing to this clinical entity. Circ Res. 2018;122(4):624–38. doi:10.1161/CIRCRESAHA.117.311586
2. Sun H, Saeedi P, Karuranga S, Pinkepank M, Ogurtsova K, Duncan BB, et al. IDF diabetes atlas: global, regional and country-level diabetes prevalence estimates for 2021 and projections for 2045. Diabetes Res Clin Pract. 2022;183:109119. doi:10.1016/j.diabres.2021.109119. Epub 2021 Dec 6. Erratum in: Diabetes Res Clin Pract. 2023 Oct;204:110945. doi:10.1016/j.diabres.2023.110945. PMID: 34879977; PMCID: PMC11057359.

3. Zheng H, Yang Z, Xin Z, Yang Y, Yu Y, Cui J, et al. Glycogen synthase kinase-3β: a promising candidate in the fight against fibrosis. Theranostics. 2020;10(25):11737-53. doi:10.7150/thno.47717. PMID: 33052244; PMCID: PMC7545984.
4. Parim B, Sathibabu Uddandrao VV, Saravanan G. Diabetic cardiomyopathy: molecular mechanisms, detrimental effects of conventional treatment, and beneficial effects of natural therapy. Heart Fail Rev. 2019;24(2):279–99. doi:10.1007/s10741-018-9749-1
5. Lorenzo-Almorós A, Cepeda-Rodrigo JM, Lorenzo Ó. Diabetic cardiomyopathy. Rev Clin Esp. 2022;222(2):100–11. doi:10.1016/j.rceng.2019.10.012
6. DeFronzo R, Fleming GA, Chen K, Bicsak TA. Metformin-associated lactic acidosis: current perspectives on causes and risk. Metabolism. 2016;65(2):20–9. doi:10.1016/j.metabol.2015.10.014
7. Thomas I, Gregg B. Metformin; a review of its history and future: from lilac to longevity. Pediatr Diabetes. 2017;18(1):10–6. doi:10.1111/pedi.12473
8. Hao P, Jiang F, Cheng J, Ma L, Zhang Y, Zhao Y. Traditional Chinese medicine for cardiovascular disease: evidence and potential mechanisms. J Am Coll Cardiol. 2017;69(24):2952–66. doi:10.1016/j.jacc.2017.04.041
9. Cheng X, Huang ZD. Effect of zuogui jiangtang shuxin recipe on glucose-lipid metabolism and inflammatory cytokines in high-fat diet MKR mice. Chin Tradit Herb Drugs. 2011;42(03):546–9.
10. Cheng X, Wu YJ. Protective effect of zuogui jiangtang shuxin recipe on myocardial impairment in MKR mice. Chin Tradit Herb Drugs. 2011;42(02):343–5.
11. Wang KX, Gao Y, Gong WX, Ye XF, Fan LY, Wang C, et al. A novel strategy for decoding and validating the combination principles of huanglian jiedu decoction from multi-scale perspective. Front Pharmacol. 2020;11:567088. doi:10.3389/fphar.2020.567088. PMID: 33424585; PMCID: PMC7789881.
12. Wang K, Tian J, Li Y, Liu M, Chao Y, Cai Y, et al. Identification of components in citri sarcodactylis fructus from different origins via UPLC-Q-Exactive Orbitrap/MS. ACS Omega. 2021;6(26):17045-57. doi:10.1021/acsomega.1c02124. PMID: 34250362; PMCID: PMC8264930.
13. Hopkins AL. Network pharmacology: the next paradigm in drug discovery. Nat Chem Biol. 2008;4(11):682–90. doi:10.1038/nchembio.118
14. Fernández AM, Kim JK, Yakar S, Dupont J, Hernandez-Sanchez C, Castle AL, et al. Functional inactivation of the IGF-I and insulin receptors in skeletal muscle causes type 2 diabetes. Genes Dev. 2001;15(15):1926-34. doi:10.1101/gad.908001. PMID: 11485987; PMCID: PMC312754.
15. Nair A, Morsy MA, Jacob S. Dose translation between laboratory animals and human in preclinical and clinical phases of drug development. Drug Dev Res. 2018;79(8):373–82. doi:10.1002/ddr.21461
16. Kanehisa M, Sato Y, Kawashima M, Furumichi M, Tanabe M. KEGG as a reference resource for gene and protein annotation. Nucleic Acids Res. 2016;44(D1):D457–62. doi:10.1093/nar/gkv1070
17. Ghorbani A. Mechanisms of antidiabetic effects of flavonoid rutin. Biomed Pharmacother. 2017;96:305–12. doi:10.1016/j.biopha.2017.10.001
18. Musolino V, Gliozzi M, Scarano F, Bosco F, Scicchitano M, Nucera S,et al. Bergamot polyphenols improve dyslipidemia and pathophysiological features in a mouse model of non-alcoholic fatty liver disease. Sci Rep. 2020;10(1):2565. doi:10.1038/s41598-020-59485-3. PMID: 32054943; PMCID: PMC7018973.
19. Garcia JP, Santana A, Baruqui DL, Suraci N. The cardiovascular effects of chocolate. Rev Cardiovasc Med. 2018;19(4):123–7. doi:10.31083/j.rcm.2018.04.3187
20. Maleki SJ, Crespo JF, Cabanillas B. Anti-inflammatory effects of flavonoids. Food Chem. 2019;299:125124. doi:10.1016/j.foodchem.2019.125124
21. Yu H, Chen B, Ren Q. Baicalin relieves hypoxia-aroused H9c2 cell apoptosis by activating Nrf2/HO-1-mediated HIF1α/BNIP3 pathway. Artif Cells Nanomed Biotechnol. 2019;47(1):3657–63. doi:10.1080/21691401.2019.1657879
22. Mesgari-Abbasi M, Valizadeh H, Mirzakhani N, Vahdatpour T. Protective effects of di- and tri-peptides containing proline, glycine, and leucine on liver enzymology and histopathology of diabetic mice. Arch Physiol Biochem. 2022;128(1):59–68. doi:10.1080/13813455.2019.1662453
23. Ramezani Ali Akbari F, Badavi M, Dianat M, Mard SA, Ahangarpour A. Gallic acid improves oxidative stress and inflammation through regulating micrornas expressions in the blood of diabetic rats. Acta Endocrinol. 2019;15(2):187–94. doi:10.4183/aeb.2019.187

24. Ren Y, Tao S, Zheng S, Zhao M, Zhu Y, Yang J, et al. Salvianolic acid B improves vascular endothelial function in diabetic rats with blood glucose fluctuations via suppression of endothelial cell apoptosis. Eur J Pharmacol. 2016;791:308-315. doi:10.1016/j.ejphar.2016.09.014. Epub 2016 Sep 8. PMID: 27614127.
25. Runtuwene J, Cheng KC, Asakawa A, Amitani H, Amitani M, Morinaga A, et al. Rosmarinic acid ameliorates hyperglycemia and insulin sensitivity in diabetic rats, potentially by modulating the expression of PEPCK and GLUT4. Drug Des Devel Ther. 2016;10:2193-202. doi:10.2147/DDDT.S108539. PMID: 27462144; PMCID: PMC4940010.
26. An T, Zhang J, Lv B, Liu Y, Huang J, Lian J, et al. Salvianolic acid B plays an anti-obesity role in high fat diet-induced obese mice by regulating the expression of mRNA, circRNA, and lncRNA. PeerJ. 2019;7:e6506. doi:10.7717/peerj.6506. PMID: 30842902; PMCID: PMC6397762.
27. Li L, Li R, Zhu R, Chen B, Tian Y, Zhang H, et al. Salvianolic acid B prevents body weight gain and regulates gut microbiota and LPS/TLR4 signaling pathway in high-fat diet-induced obese mice. Food Funct. 2020;11(10):8743-8756. doi:10.1039/d0fo01116a. PMID: 32955050.
28. Rajesh KG, Suzuki R, Maeda H, Yamamoto M, Yutong X, Sasaguri S. Hydrophilic bile salt ursodeoxycholic acid protects myocardium against reperfusion injury in a PI3K/Akt dependent pathway. J Mol Cell Cardiol. 2005;39(5):766–76. doi:10.1016/j.yjmcc.2005.07.014
29. Dhanasekaran A, Gruenloh SK, Buonaccorsi JN, Zhang R, Gross GJ, Falck JR, et al. Multiple antiapoptotic targets of the PI3K/Akt survival pathway are activated by epoxyeicosatrienoic acids to protect cardiomyocytes from hypoxia/anoxia. Am J Physiol Heart Circ Physiol. 2008;294(2):H724-35. doi:10.1152/ajpheart.00979.2007. Epub 2007 Nov 30. PMID: 18055514; PMCID: PMC2443685.
30. Ebner B, Lange SA, Hollenbach D, Steinbronn N, Ebner A, Fischaleck C, et al. In situ postconditioning with neuregulin-1β is mediated by a PI3K/Akt-dependent pathway. Can J Cardiol. 2015;31(1):76-83. doi:10.1016/j.cjca.2014.10.035. Epub 2014 Nov 6. PMID: 25547554.
31. Kim D, Dan HC, Park S, Yang L, Liu Q, Kaneko S, et al. AKT/PKB signaling mechanisms in cancer and chemoresistance. Front Biosci. 2005;10:975-87. doi:10.2741/1592. PMID: 15569636.
32. Niu F, Qian K, Qi H, Zhao Y, Jiang Y, Sun M. Antiapoptotic and anti-inflammatory effects of CPCGI in rats with traumatic brain injury. Neuropsychiatr Dis Treat. 2020;16:2975–2987. doi:10.2147/NDT.S281530
33. Opferman JT, Kothari A. Anti-apoptotic BCL-2 family members in development. Cell Death Differ. 2018;25(1):37–45. doi:10.1038/cdd.2017.170
34. Mallipattu SK, Gallagher EJ, LeRoith D, Liu R, Mehrotra A, Horne SJ, et al. Diabetic nephropathy in a nonobese mouse model of type 2 diabetes mellitus. Am J Physiol Renal Physiol. 2014;306(9):F1008-17. doi:10.1152/ajprenal.00597.2013. Epub 2014 Mar 5. PMID: 24598803; PMCID: PMC4010680.
35. Rena G, Lang CC. Repurposing metformin for cardiovascular disease. Circulation. 2018;137(5):422–4. doi:10.1161/CIRCULATIONAHA.117.031735
36. Fung CS, Wan EY, Wong CK, Jiao F, Chan AK. Effect of metformin monotherapy on cardiovascular diseases and mortality: a retrospective cohort study on Chinese type 2 diabetes mellitus patients. Cardiovasc Diabetol. 2015;14:137. doi:10.1186/s12933-015-0304-2
37. Zhang J, Huang L, Shi X, Yang L, Hua F, Ma J, et al. Metformin protects against myocardial ischemia-reperfusion injury and cell pyroptosis via AMPK/NLRP3 inflammasome pathway. Aging (Albany NY). 2020;12(23):24270-87. doi:10.18632/aging.202143. Epub 2020 Nov 24. PMID: 33232283; PMCID: PMC7762510.
38. Higgins L, Palee S, Chattipakorn SC, Chattipakorn N. Effects of metformin on the heart with ischaemia-reperfusion injury: evidence of its benefits from in vitro, in vivo and clinical reports. Eur J Pharmacol. 2019;858:172489. doi:10.1016/j.ejphar.2019.172489